Biochemical Engineering Journal 167 (2021) 107897

Contents lists available at ScienceDirect

Biochemical Engineering Journal

journal homepage: www.elsevier.com/locate/bej

Characterization of dynamic regulation in Chinese hamster ovary (CHO) cell cultures in the late exponential phase

Sha Sha [a], Bingyu Kuang [b], Seongkyu Yoon [a,b,*]

[a] Biomedical Engineering and Biotechnology, University of Massachusetts Lowell, Lowell, MA, 01854, USA
[b] Chemical Engineering, University of Massachusetts Lowell, Lowell, MA, 01854, USA

ARTICLE INFO

Keywords:
CHO cell culture
Transcriptomics
Oxidative stress
RNA-Seq
Dynamic regulation
Exponential growth

ABSTRACT

Chinese hamster ovary (CHO) cells are the most commonly used host cells to produce biologics in the biopharmaceutical industry. In a batch or fed-batch process, cells grow at a relatively constant rate at the exponential growth phase, a period that is commonly assumed as a "metabolically quasi steady-state". However, the cell culture environment, such as medium composition, does not maintain the same during this time; instead, the medium composition changes with nutrient decrease, cell density increase, and byproduct accumulation. Therefore, cellular microenvironment may respond to such process changes. This study examined the transcriptome across the late exponential growth phase of three CHO cell lines to illuminate the dynamic regulation at glycolysis, tricarboxylic acid (TCA) cycle, glycosylation, and antioxidant pathways. We found that the expression of a series of genes has a concurrent shift around 91 h, coincident with lactate shift from its accumulation to consumption. The gene expressions altogether suggest a homeostasis behavior before the 91 h, presumably a response to the high abundance of nutrients at the exponential growth phase.

1. Introduction

As the main workhorse in the biopharmaceutical industry, Chinese hamster ovary (CHO) cells are the most used host cells to produce various biologics, including monoclonal antibodies (mAbs). During the exponential phase in a batch or fed-batch process, the environment of cell culture changes with nutrient depletion, cell density increase, byproduct accumulation, and so on. At the same time, cells maintain a rapid and relatively constant growth rate. Cellular physiology at such a growing stage under the changing environment has not been well understood.

There is clear evidence that the cellular activities are modulated by various pathways which are also connected with each other. For example, previous studies have shown the connections between apoptosis, lactate, and pyruvate metabolism [1], glycosylation and oxidative potential [2], oxidative stress and glycolysis, nucleotide sugar synthesis and sialylation [3]. A broader view of CHO cell global microenvironment has been enabled by using omics approaches [4–11]. In particular, the RNA-Seq technology has contributed to a comprehensive evaluation of cellular metabolism at the transcription across diverse pathways [10,12–17].

Many studies have examined the cellular regulations across the transition from the cell culture exponential to the stationary phase, for which the changes are usually dramatic [18–22]. The exponential phase has been commonly assumed as a "pseudo-steady state" when cells maintain rapid growth, and the physiological status is expected to be minimally changed. Previous studies have characterized the dynamics of CHO cell genome and epigenome across the exponential and stationary phase in batch culture [23] and explored the dynamics of histone modification and gene expression in an entire batch culture for a non-producer cell line [24]. However, the transcriptomic regulation focusing on the exponential phase for mAb-producing CHO cell lines has not been performed.

Here, we investigated the transcriptomic dynamics of three mAb-producing CHO cell lines at the late exponential phase and explored the potential cellular adaption during this stage. In the present work, the studied pathways include the central metabolism, N-linked glycosylation, and the redox environment. As a consensus of the three cell lines, we found a shift of transcriptome with genes regulated from various pathways at 91 h of cell culture. Based on our observations, we formed a picture of homeostatic efforts that cells may experience during the late exponential phase.

* Corresponding author at: 1 University Ave, Lowell, MA, 01854, USA.
E-mail address: Seongkyu_Yoon@uml.edu (S. Yoon).

https://doi.org/10.1016/j.bej.2020.107897
Received 30 June 2020; Received in revised form 7 December 2020; Accepted 11 December 2020
Available online 27 December 2020
1369-703X/

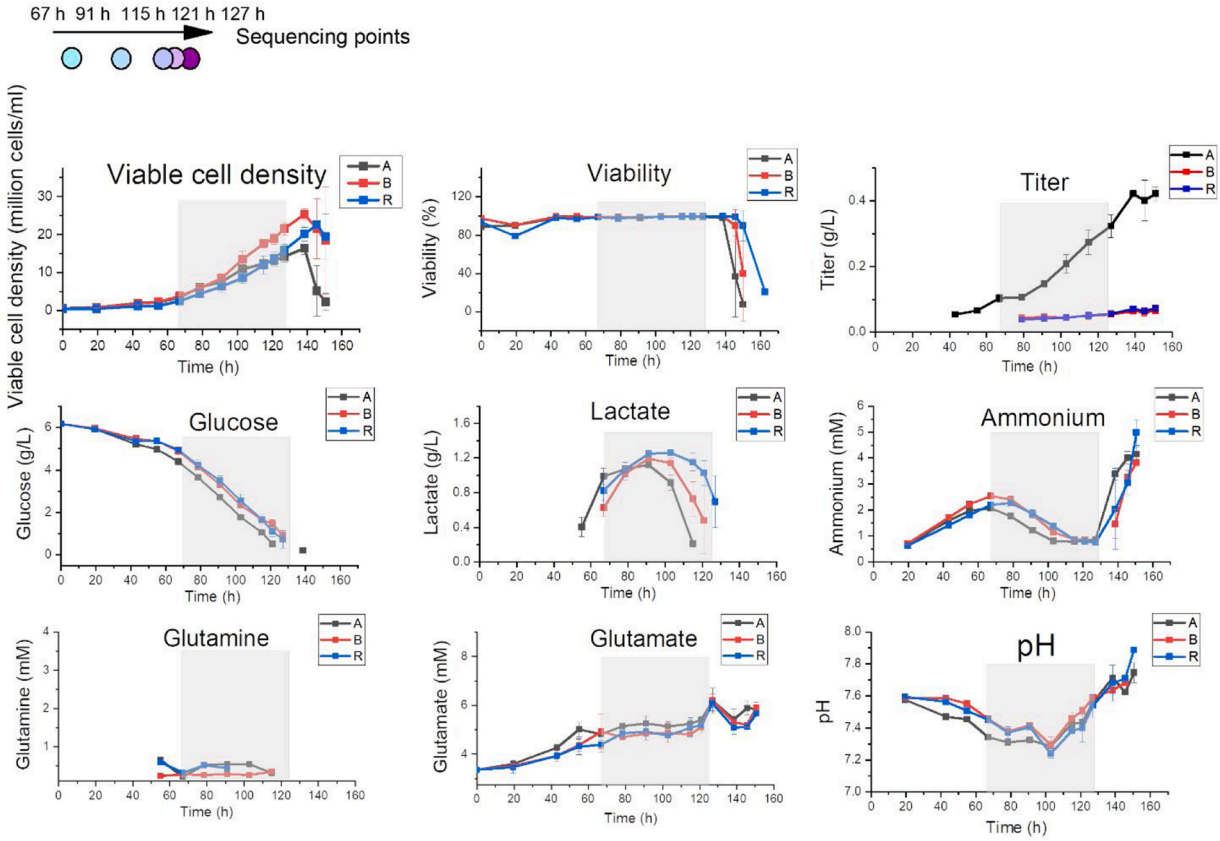

Fig. 1. Cell growth, mAb titer, metabolites and pH profiles of cell line A, B and R batch cultures. The error bars shown in the data indicate the variation from the three replicate cultures.

2. Methods

2.1. Cell culture

The three GS−CHO cell lines used in this study were donated by industrial collaborators. Cells were parented from CHO-S and engineered to respectively produce Adalimumab, Bevacizumab, and Rituximab biosimilars (each cell line was respectively called A, B, and R in the study). Cells were thawed and proceeded in a seed culture until reaching the exponential phase. Cells were then inoculated at a density of 0.3 million per ml in 250 mL shake flasks with 50 mL working volume. Each cell line was cultured with triplicate flasks and in a batch mode at 37 °C, 5% CO_2, and 125 rpm incubator. CD-Forti CHO media (ThermoFisher Scientific, Waltham, MA) was used for all cultures without glutamine supplementation.

2.2. Cell culture analysis

Cells were counted by Cedex Hires Analyzer (Roche Life Science, Indianapolis, IN). Extracellular metabolites, including glucose, lactate, ammonia, and glutamate, were measured using the Nova Profile analyzer (Nova Biomedical, Waltham, MA). Mab titer was determined by Waters Alliance 2695 high-performance liquid chromatography system (HPLC) (Waters, Milford, MA) in alliance with POROS® A 20 μm column (Thermo Fisher Scientific, Waltham, MA).

2.3. RNA extraction

Approximately 5 million cells were stored in RLT buffer (Qiagen, Germantown, MD) and saved at -80 °C. The total RNA was extracted using the RNeasy mini kit (Qiagen, Valencia, CA) following the manufactures' instructions and quantified using Qubit Fluorometer (ThermoFisher Scientific, Waltham, MA). The integrity values of the extracted RNA were examined by the Bioanalyzer (Agilent Technologies, Santa Clara, CA).

2.4. RNA-Seq and data processing

The mRNA was extracted from total RNA and converted to cDNA with dual indexes using Illumina mRNA stranded library preparation kit (Illumina, San Diego, CA). The cDNA libraries were loaded onto the high output flow cells and sequenced by the NextSeq 500 (Illumina, San Diego, CA). The fastq data were uploaded to Massachusetts Green High Performance Computing Center (GHPCC) and processed via Dolphin, an online data analysis interface developed by UMass medical school (https://dolphin.umassmed.edu/). The analysis pipeline performed a data quality check and then an alignment of the short reads to a reference database using RSEM. The details of the pipeline could be found in a previous publication [10]. The RSEM produces two types of counts: estimated counts (non-normalized) and the normalized values of transcript per million reads (tpm). These two forms of data were respectively used in the differential gene analysis and the genes' dynamic profiles.

2.5. Transcriptomic data analyses

Principal component analysis (PCA) and differential expression gene (DEG) analysis were performed using the built-in tools in Debrowser [25]. The gene list with the most varied 1000 genes was used as inputs in the PCA. DEG analysis was conducted by DESeq2 using the expected counts from RSEM as inputs. A threshold of p-adj < 0.01 (Benjamini--Hochberg process) was applied in the significance of analysis. The expression data of genes associated with particular pathways were extracted from the gene expression results using an R-based Bioconductor "mygene" package. The data normalized to tpm were used to

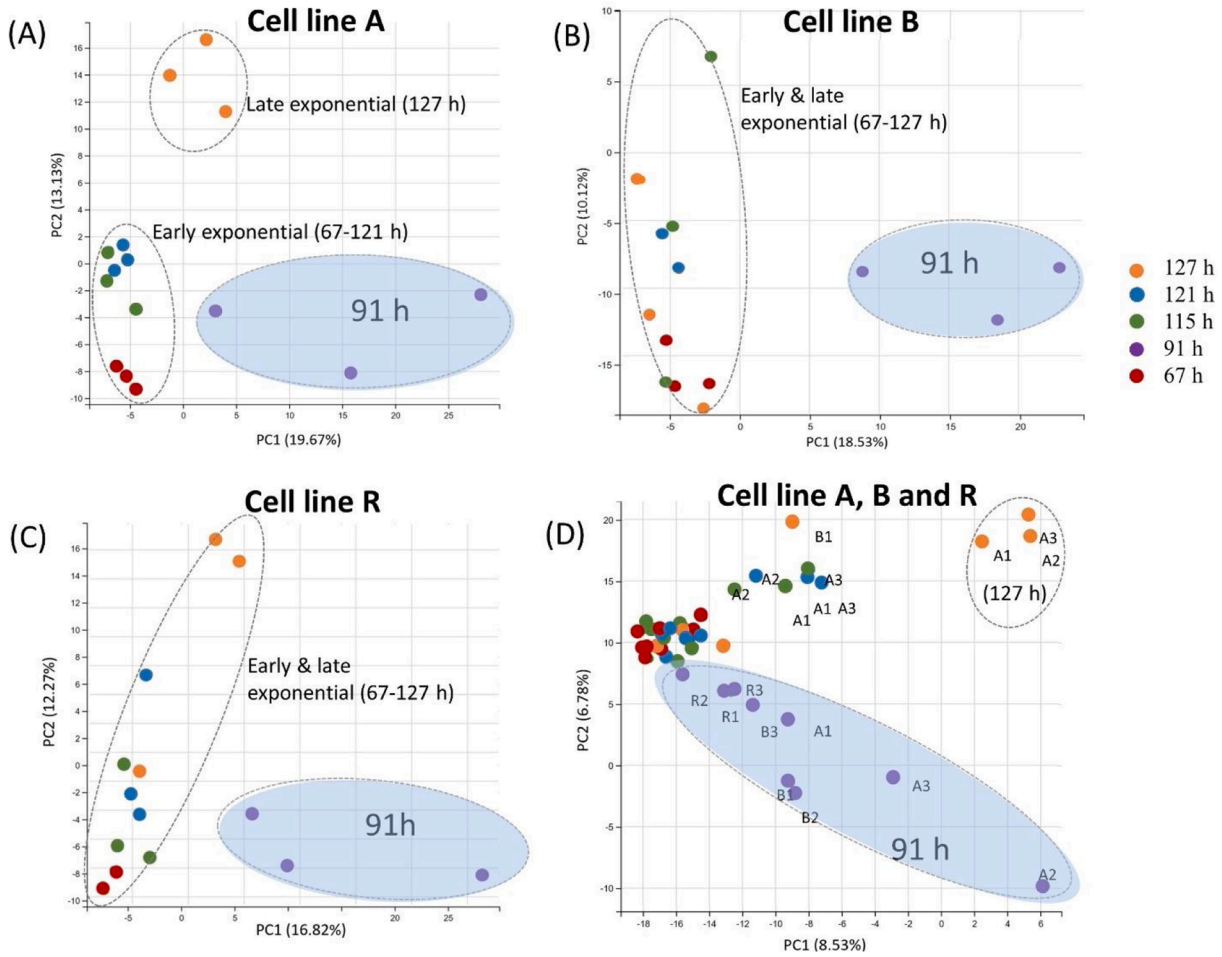

Fig. 2. Principal component analysis (PCA) of time-series gene expression data. The patterns are shown for (A) cell line A; (B) cell line B, (C) cell line R, and (D) combination of cell line A, B and R. Each circle indicates a cluster. The blue circles indicate a distinct transcriptomic status at 91 h.

analyze the dynamic trends of gene expressions. GO functions of gene sets were conducted using a web-based tool Gorilla [26].

3. Results

3.1. Cell culture

The culture of three cell lines A, B, and R were conducted for 150 h in triplicates (Fig. 1). All the cultures maintained more than 90 % viability before 140 h. For all the three cell cultures, the glucose was constantly consumed. Lactate shifted from accumulation to consumption at 91 h. The pH varied within a range of 7.2 and 7.6; its first decrease was concurrent with lactate accumulation while the subsequent increase was concurrent with lactate consumption. The ammonia and glutamate fluctuated throughout the culture. The glutamine was maintained at a low level near the instrument's detection limit.

It was observed that cell line A had different cell growth and mAb production profiles from cell line B and R. Specifically, cell line A started to decrease growth around 103 h (shown in the black line), while the other two cell lines maintained the initial growth rates (shown in the red and blue lines). Interestingly, cell line A was a relatively high producer than cell line B and R. It was known from our earlier study by comparing the transcriptome between the cell line A (high producer) and the other two cell lines (low producers) that cell line A needed additional energy to support mAb production [10]. Therefore, cell line A was confronted with a faster depletion of nutrients in the medium including glucose, an earlier shift of lactate from production to accumulation as compared to the other two cell lines, and a faster decline of growth rate (Fig. 1).

Because seed cells were initially maintained at the exponential phase, there was no lag phase of cells in the present cultures. Here, we considered 60–130 h to be a late exponential phase for the three cultures (as shaded in Fig. 1) and studied the cell transcriptome changes across this period. The behavior of the biological replicates within this period was consistent, as only subtle variations were seen within the replicated cultures. Cell mRNA was extracted and sequenced at five dynamic time points: 67, 91, 117, 121, and 127 h.

3.2. Cluster analysis of the time-series global transcriptome

We first analyzed the global transcriptomic data, including the replicated cultures, using PCA. The analysis clustered five different time points according to the similarity shown in the transcriptome.

Fig. 2**A to C** individually show the PCA of the three cell lines A, B, and R. For cell line B and R (Fig. 2**B** and C), a dynamic trend moved in the plots from the bottom to the top, but overall forming one cluster that blends the late and early time points (dashed circle), except for 91 h (highlighted in a blue circle). Accordingly, no gene ontology (GO) functions were enriched by comparing among 67, 117, 121, and 127 h, indicating the transcriptome's similarities within the cluster. In contrast, cell line A had a clear separation between the last time point (127 h) and any earlier time points, forming two distinct clusters (dashed circles) (Fig. 2A). Between 121 and 127 h, a GO function corresponding to negative regulation of mitotic sister chromatid cohesion maintenance was enriched from the differentially expressed genes (altered greater than 1.4-fold, p-adj<0.01). This transcriptomic change corresponded to the decrease of cell growth.

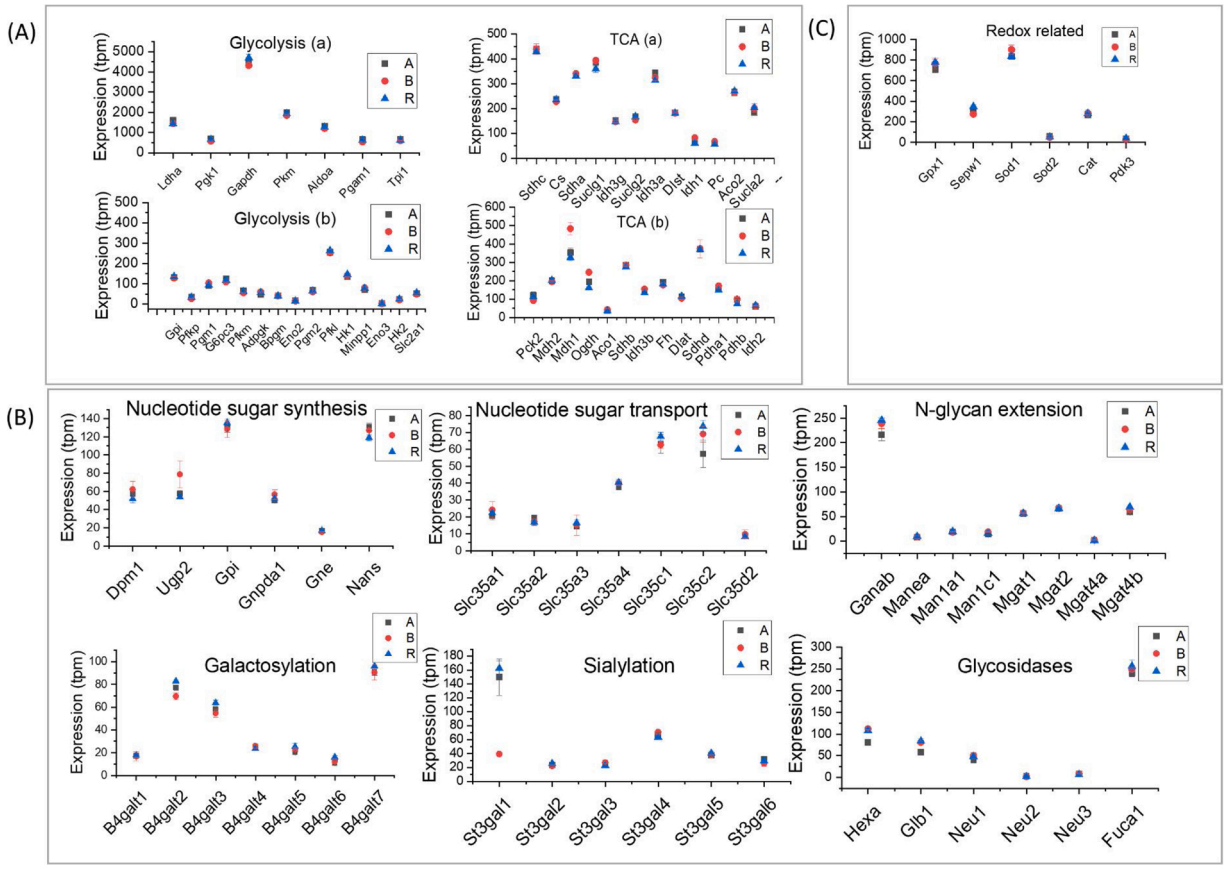

Fig. 3. A landscape of the expression level at 67 h (first time point sequenced) for the genes from the pathways of (A) glycolysis and TCA; (B) glycosylation-related, including nucleotide sugar synthesis, nucleotide sugar transport, N-glycan extension, galactosylation, sialylation, and glycosidase activity; (C) redox-related. The values of gene expression are presented by transcript per million reads (tpm) as described in the method 2.4. Error bars are shown for the variation from the three replicate cultures.

Notably, we found a distinct cluster at 91 h from all the three cultures (blue circles in Fig. 2**A-2C**). This unique cluster indicates a transcriptomic shift from 67 h to 91 h, followed by a change to the previous status after 91 h. To verify the findings from individual cell lines, we conducted PCA by combining all the three cell lines' data (Fig. 2D). The analysis confirmed the distinction found in the late culture A (dashed circle) and the distinct separation of 91 h for all the cultures (highlighted in blue). In the following analyses with specific pathways, we identified a series of genes that showed shifted expression across 91 h.

3.3. A landscape of gene expression level

To understand the gene expression abundance, we provided a landscape of gene expression in the pathways of glycolysis, TCA, redox, and glycosylation at the first time point 67 h (Fig. 3). The full names of these genes are available in **Table S1**. We found that the genes in the central metabolism, such as glycolysis and TCA, generally acquired high expressions (Fig. 3A). The most highly expressed glycolysis genes were *Ldha*, *Pgk1*, *Gapdh*, *Pkm*, *Aldoa*, *Pgam1,* and *Tpi1*, with several thousand tpm in expression (shown in glycolysis (a)). Relatively, the glycosylation pathway genes showed lower expressions, generally below one hundred tpm (Fig. 3B). The antioxidant enzyme genes were also highly expressed, ranging from a few hundred to one thousand tpm (Fig. 3C). This general landscape of gene expressions is consistent among the three cell lines.

3.4. Time-course gene expression in the energy pathways

We then evaluated the time-course gene expression in the energy pathways, mainly the glycolysis and TCA pathways as shown in Fig. 4**A.** The full names of the metabolites are available in **Table S2.** The dynamic expressions of the genes in the metabolic network were plotted **(**Fig. 4**)**. The group includes 22 glycolytic genes/isoforms in Fig. 4B, and 25 expressed TCA genes/isoforms in Fig. 4**C.** Data at each time point were normalized to the expression at 67 h.

The dynamic changes in the gene expression were mostly smaller than two-fold. The majority of the glycolytic genes showed decreased expression over time (Fig. 4**B-i**), which applied to many highly-expressing glycolytic genes. One decreasing gene was the *Pkm* gene, which encodes pyruvate kinase – a rate-limiting enzyme in the glycolysis. On the other hand, only a few genes showed increased expression (Fig. 4**B-iii**), including the glucose intake transporter Glut1 *(Slc2a)*. Some other glycolytic genes increased expression before 91 h, followed by a decrease afterward, forming an expression shift surrounding 91 h (Fig. 4**B-ii**, highlighted in blue). These genes showing a shifted pattern are separately summarized in Table 1 and will be discussed in section 4.2.

Similarly, most of the TCA genes showed a decrease in expression which began at 67 h or 91 h (Fig. 4**C-i**) and a small number of genes showed an increase in expression (Fig. 4**C-iii**). One of these increasingly expressed was the *glul* gene that encodes glutamine synthetase for glutamine synthesis, which was also highly expressed. To the opposite, the *gls* gene that encodes glutaminase for degrading glutamine into glutamate and ammonium was expressed minimally. The pattern of *glul* and *gls* gene agrees with the metabolic phenotype shown in Fig. 1, where ammonia was consumed while glutamate level remained stable, possibly indicating cellular usage of ammonia and glutamate to synthesize glutamine during the late exponential phase.

Pyruvate is an essential node in the transition between glycolytic and

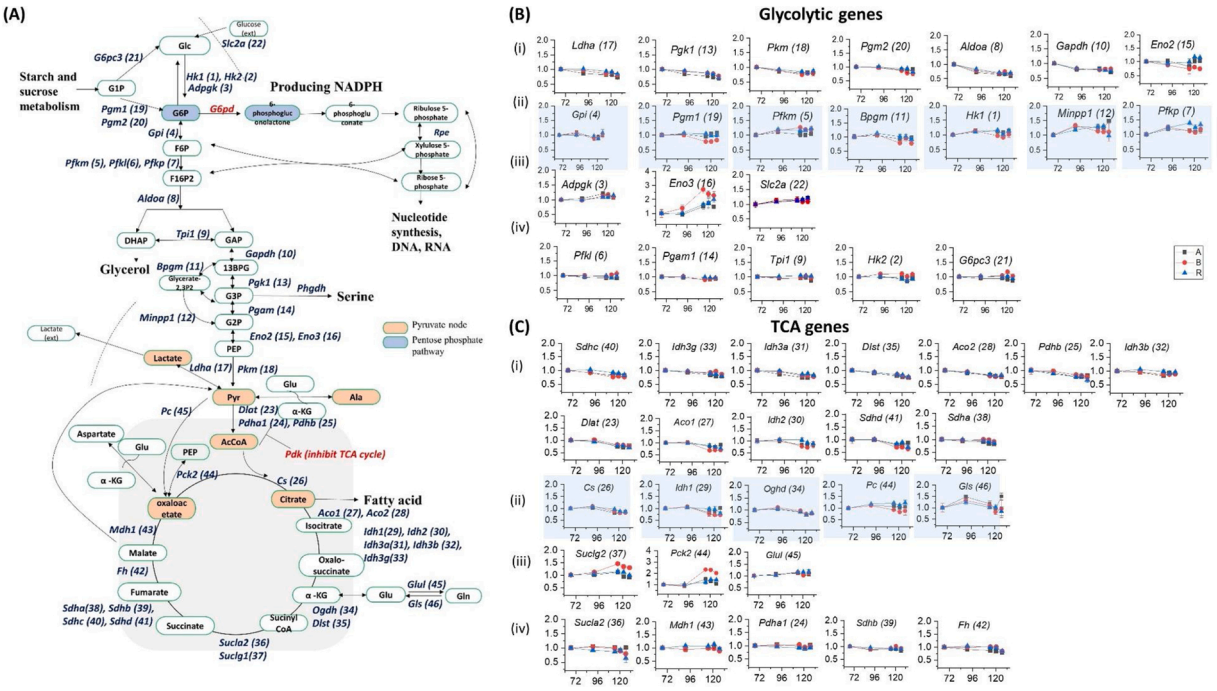

Fig. 4. The gene expression in the cell central metabolism. (A) A network of glycolysis, TCA and pentose phosphate pathways. The full names of genes and metabolites are given in Table S1 - S2. (B) Time series expression of genes at glycolysis. (C) Time-series expression of genes at TCA. The genes presented in (B) and (C) are categorized into four groups of trends (i) decreasing; (ii) increasing followed by decreasing (a shift); (iii) increasing; (iv) no clear trends. The genes showing a shift at 91 h are also highlighted in a blue shade. Data at each time point are normalized to the expression at 67 h. Error bars are shown for the variation from the three replicate cultures.

TCA fluxes. Therefore, the branches of pyruvate distribution and the genes associated with in- and out-fluxes of pyruvate were of interest (shown in **Fig. S1**). Over time, the expression of *Pkm* (producing pyruvate from glycolysis) was decreased, while the *Pck2* (producing pyruvate from TCA) was increased. The change of these two genes suggests a reduced flow into pyruvate from glycolysis, whereas an increased flow replenishing from TCA to pyruvate. Especially, the increase of *Pck2* after 91 h for cell line B, which was the fastest-growing cells, was the most prominent (more significant than 2-fold).

3.5. Time-course gene expression in the glycosylation pathways

Next, we analyzed fifty-four glycosylation genes that were identified in previous literature, involving the glycosylation steps of nucleotide sugar synthesis, nucleotide sugar transport, glycan extension, galactosylation, sialylation, fucosylation, and degradation [18]. We plotted the dynamic gene expressions normalized to the first time point by seven groups, each representing one glycosylation step in Fig. 5. A total of forty-three genes were expressed in our data. These genes mostly showed mild changes (< 2-fold) over time. Interestingly, several genes showed a shift at 91 h, as highlighted in blue from almost every step of the glycosylation process, summarized in Table 1. The degree of the change was as large as nearly two-fold. We found that almost every glycosidase showed an increase in expression dynamically except Neuraminidase 3 (*Neu3*) (Fig. 5G).

3.6. Time-course gene expression associated with the redox environment

In the redox system, enzymes in the antioxidant network are responsible for different roles and maintain balance [27]. We examined the dynamics of several major enzymes in the antioxidative enzyme systems, which are glutathione peroxidase (*Gpx*), superoxide dismutase (*Sod*), gene catalase (*Cat*), and several other genes known to be associated with the redox environment (Fig. 6).

Several genes showed decreased expression, including the *Gpx1* gene that encodes one of the most critical antioxidant enzymes for cell protection from oxidative stress damage. Another gene showing decreased expression was Selenoprotein W 1 (*Sepw1*), encoding a selenoprotein of redox function. Notably, these two genes (*Gpx1* and *Sepw1*) had a decrease by more than two-fold (p-adj <0.01), which was the highest degree of variation over a 24 h interval in the transcriptome. Another pair of genes, the *Sod1* (one isoform gene of *Sod*) and the regulatory *p53* gene with a role in antioxidative stress activity associated with glutathione peroxidase, also showed a decrease in expression.

Several redox-related genes showed a shift at 91 h (highlighted in blue, Fig. 6). These include two antioxidative genes *Sod2* and *Cat,* and several redox environment- associated genes, including (1) *Hif1α,* which encodes a primary unit of hypoxia-inducible factor, a transcriptional factor ubiquitously expressed in response to oxidative stress; (2) *Pdk3*, which encodes an isoform of pyruvate dehydrogenase kinase that inhibits pyruvate dehydrogenase, enhances glycolytic and inhibits TCA pathways; (3) *G6pd,* which encodes glucose-6-phosphate dehydrogenase, an enzyme converting G6P to pentose phosphate pathway (PPP); (4) *Casp3,* which encodes caspase 3 and is responsible for apoptosis regulation.

4. Discussion

4.1. Insights into the dynamics of central metabolism, glycosylation, and redox regulation

Over the late exponential course, the central metabolism and glycosylation pathways underwent generally less than 2-fold change. This indicates a milder change in the transcriptome during the late exponential phase compared to the transition from the exponential to the stationary phases [12,24]. The gene expression pattern among the three cell lines was mostly similar. A unique alteration in the transcriptome, linked with DNA replication, was identified in cell line A

Table 1
The list of genes shifting expression at 91 h.

Genes	Function
Glycolysis	
Gpi	Glucose-6-phosphate isomerase
Pgm1	Phosphoglucomutase 1
Pfkm	Phosphofructokinase, muscle
Bpgm	Bisphosphoglycerate Mutase
Hk1	Hexokinase 1
Minpp1	2,3-Bisphosphoglycerate 3-Phosphatase
Pfkp	Phosphofructokinase, platelet
TCA	
Cs	Citrate synthase
Idh1	Isocitrate dehydrogenase
Oghd	Oxoglutarate (alpha-ketoglutarate) dehydrogenase-like
Pc	Pyruvate carboxylase
Gls	Glutaminase
Glycosylation synthesis	
Ugp2	UDP-Glucose pyrophosphorylase; G1P + UTP - > UDP-Glc
Dpm1	Dolichyl-phosphate mannosyltransferase subunit 1
Mannose trimming	
Manea	Mannosidase endo-alpha
Man1c1	Mannosyl-oligosaccharide 1,2-alpha-mannosidase
Nucleotide sugar transport	
Slc35a1	CMP-sialic acid transporter
Slc35d2	UDP-GlcNAc/UDP-Glucose transporter
Galactosylation	
B4galt1	Beta-1,4-Galactosyltransferase 1
B4gat5	Beta-1,4-Galactosyltransferase 5
Sialylation	
St3gal1	ST3 Beta-Galactoside Alpha-2,3-Sialyltransferase 1
St3gal6	ST3 Beta-Galactoside Alpha-2,3-Sialyltransferase 6
Fucosylation	
Fut8	Fucosyltransferase 8
Oxidative regulation	
Hif1α	Hypoxia induced factor 1a
Pdk3	Pyruvate dehydrogenase kinase
Casp3	Caspase-3
G6pd	Glucose-6-phosphate dehydrogenase
SOD2	Superoxide dismutase 1, soluble, Mn dependent, in mitocondria
Cat	Catalase, transcript variant X1

when it underwent a growth-declining stage.

We found that the dynamic behaviors of gene expression in the glycolysis and TCA are consistent with many existing understandings [28,29] and could be aligned with cellular behaviors previously investigated from the metabolic point of view. First, we identified that the expression of several glycolytic genes was significantly higher than TCA genes. Consistently, the fluxes in the glycolytic pathways were larger than TCA for CHO cells, known as the "Warburg Effect" [30]. Second, most glycolytic and TCA genes showed a decrease in expression throughout the late exponential phase, overall in agreement with other studies that showed decreased metabolic fluxes [31,32]. Finally, the genes surrounding pyruvate indicate increased fluxes to the TCA cycle as cultures progress, in agreement with a previous study that showed shifted fluxes from glycolysis to TCA metabolism over time [33].

A surprising finding from the glycosylation pathways was the increased expression of the glycosidases that catalyze glycan degradation. It has been reported that glycosidase expression could increase at the stationary phase, possibly due to the ammonia accumulation [21]. However, the increased expression of glycosidase in the late exponential phase was not previously reported and may require more investigations in the context of glycosylation control [20].

The gene *Sepw1* and *Gpx1* were among the most significantly decreasing genes in the transcriptome, both with a decrease of more than two-fold. Both genes are related to the redox system: besides the antioxidant role of *Gpx1* gene, the *Sepw1* gene encodes a selenoprotein that is regulated in redox-related processes. The gene *p53* – which plays a role in regulating apoptosis and antioxidative stress activity – also showed a co-decrease in expression. We hypothesized that the regulation shown with p53 and Gpx could be associated, as studies found human *Gpx* promoter regions include a consensus binding sequence of p53 [34,35].

4.2. Regulatory microenvironment at 91 h

From the PCA of the global transcriptome, we identified a transition of cellular status at 91 h. Interestingly, Hernandez et al.'s study also revealed a shift of gene expression at the exponential phase with a non-producing CHO-K1 cell line, a different lineage from our study [24]. In this work, we used three cell lines producing different mAbs, and the results show that the transcriptomic shift is a general feature across cell lines producing different mAbs. Therefore, the transcriptomic shift could be a general behavior of CHO cell lines independent from mAb production. After finding the global transcriptome pattern, we identified concomitant shifts of genes in various pathways, which in common increased before 91 h and then decreased after 91 h (as summarized in Table 1). We propose that this state change is associated with homeostatic efforts within the redox environment, plausibly triggered by the high abundance of nutrients at the initial culture. Excess nutrients could cause excessive mitochondria oxidative metabolism and raise oxidative stress [36]. At the beginning of cell culture when glucose is abundant, CHO cells can take excess glucose. Then, oxidative metabolism and reactive oxygen species (ROS) production primarily occur in the mitochondria [37]. We hypothesized that cells might carry out a short-term regulation to mitigate such upcoming stress in TCA by regulating antioxidative enzymes and upregulating glycolysis. Correspondingly, such regulation could be eliminated after 91 h after glucose abundance was decreased and the pressure on TCA activity was released.

With our hypothesis (as shown in Fig. 7), a series of genes elevated expression temporarily before 91 h to combat the oxidative stress in the mitochondria TCA metabolism. Firstly, the increased expression of *Sod2* and *Cat* genes encoding antioxidant enzymes before 91 h might have been a direct regulation of the redox environment. Simultaneously, the expression of *Hif1α* gene was elevated before 91 h; this gene encodes a transcriptional factor for a series of cellular metabolism regulation in response to oxidative stress [28]. The *Pdk* gene also showed increased expression, probably under the effect of *Hif1*, to encode pyruvate dehydrogenase kinase to enhance glycolysis and inhibit TCA, a regulation known to mitigate ROS production in the mitochondria [28,38]. The *G6pd* gene expressing glucose-6-phosphate dehydrogenase was also increased before 91 h. The G6pd is a rate-limiting enzyme for converting glycolysis to oxidative PPP. As NADPH produced in PPP pathway regulates oxidative stress [39], the G6pd regulation could have been triggered to control the NADPH abundance [34]. Besides *Pdk* and *G6pd* genes, several glycolytic and TCA genes were also temporarily increased at 91 h. Even though these changes were at a small degree, they could contribute to the regulation associated with the redox environment.

Besides the energy pathways, other pathways might also be linked to the regulation before 91 h. An apoptosis *Casp3* gene for encoding caspase was increased before 91 h, reflecting the effects of oxidative stress on apoptosis and autophagy as previously reported [40]. The co-shift of many genes from glycosylation pathways, including the genes for synthesizing glycan precursors (especially with mannose, N-acetylglucosame, and galactose), transporting glycan precursors from the cytoplasm to Golgi, and glycan extension, is in line with previous reports about the hypoxic effects on glycosylation [41] and shifting patterns of the glycan precursors' dynamics [42–45].

Finally, the redox regulation and lactate co-shift might be associated. Lactate shift is a common phenomenon in cell culture. Recent studies identified different metabolic states before and after the lactate shift [31–33]. The lactate shift was also linked with AKT1 signaling pathways that regulate glycolysis and redox environment [46,47]. Here, we found simultaneous changes at the transcriptome of apoptosis, hypoxia, and oxidative stress when lactate shifted, in agreement with several studies together where these pathways were evaluated separately [38,48–50]. Thus, we hypothesized that the redox microenvironment could trigger

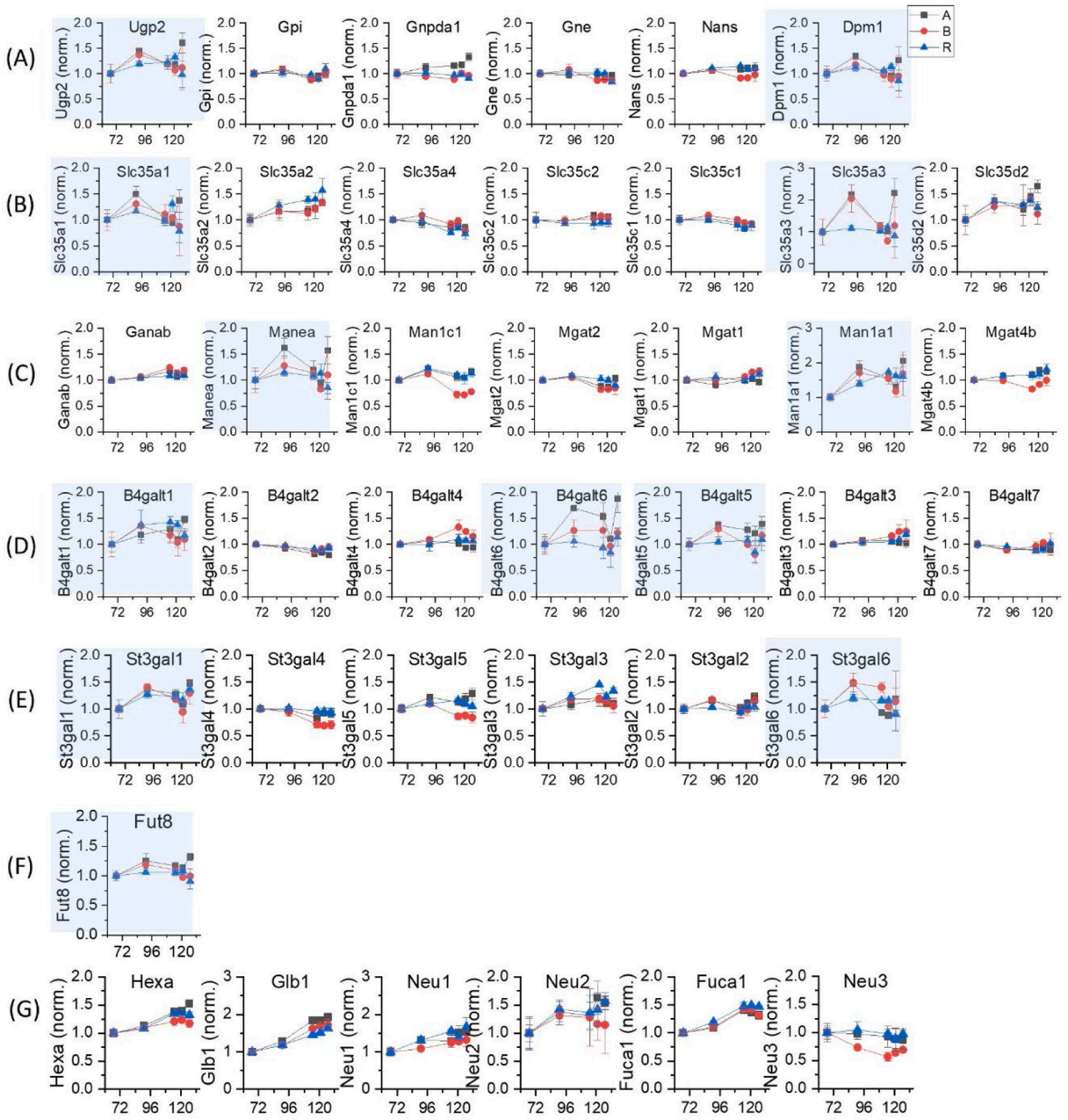

Fig. 5. Dynamic expression of the glycosylation pathway genes. (A) Nucleotide sugar synthesis; (B) Nucleotide sugar transport; (C) N-glycan extension; (D) Galactosylation; (E) Sialylation; (F) Fucosylation; (G) Glycosidases. The genes showing a shift at 91 h are highlighted in a blue shade. Data at each time point are normalized to the expression at 67 h. Error bars are shown for the variation from the three replicate cultures.

the lactate shift, as shown in Fig. 7: before 91 h, the redox regulation stimulated protective regulation by promoting glycolysis, under which the pathway produced lactate; as the oxidative stress decreased after 91 h, a series of genes shifted to decrease, resulting in TCA pathway increase and lactate consumption.

To conclude, the homeostatic effort summarized above suggests a redox-triggered regulation and the associated microenvironment. The regulation activity shows that cells can make regulations during steady growth in the late exponential phase, for adjusting the microenvironment to maintain intracellular homeostasis. Further studies with other omics approaches can testify to this hypothesis.

Author contributions

Sha S. designed the study and conducted experiments and analyses. Kuang B. conducted the verification of RNA-seq results by qRT-PCR. Yoon S. was the project PI and provided the main supervision and guidance to the research work. All the authors reviewed and approved the manuscript. The authors declare that they have no competing financial interests.

CRediT authorship contribution statement

Sha Sha: Conceptualization, Data curation, Formal analysis, Investigation, Methodology, Software, Visualization, Writing - original draft, Writing - review & editing. **Bingyu Kuang:** Methodology, Validation. **Seongkyu Yoon:** Conceptualization, Funding acquisition, Project administration, Resources, Supervision, Writing - review & editing.

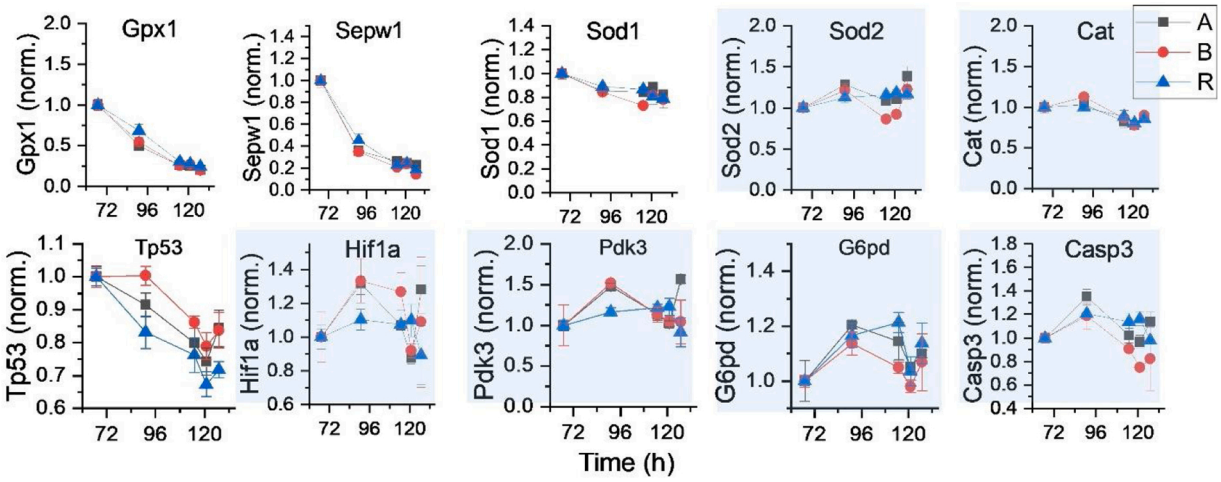

Fig. 6. Expression of the redoxrelated genes. The genes showing a shift at 91 h are highlighted in a blue shade. Data at each time point are normalized to the expression at 67 h. Error bars are shown for the variation from the three replicate cultures.

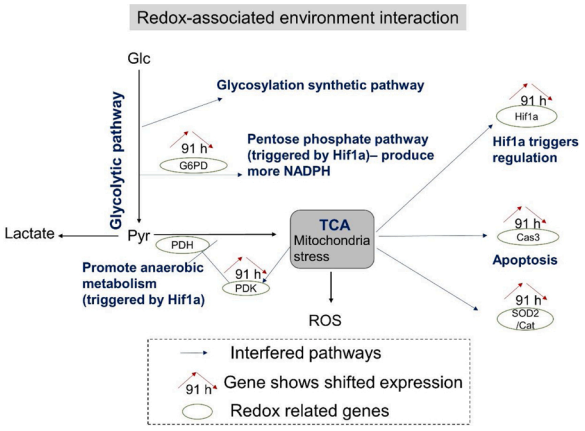

Fig. 7. An overview of the hypothetic linkages between gene regulations. The network shows a hemostatic cell microenvironment before and after 91 h.

Declaration of Competing Interest

The authors report no declarations of interest.

Acknowledgment

The study was supported by US NSF/MRI (1428272) and US NSF/IUCRC AMBIC (1624718). The authors gratefully thank Dr. Maurizio Cattaneo for providing the cell-lines, Jack Lepine from UMass Lowell Core Research Facility (CRF), and Zhuangrong Huang and Seo-young Park from Dr. Yoon's group for their participation in the work.

Appendix A. Supplementary data

Supplementary material related to this article can be found, in the online version, at doi:https://doi.org/10.1016/j.bej.2020.107897.

References

[1] N. Templeton, A. Lewis, H. Dorai, E.A. Qian, M.P. Campbell, K.D. Smith, S.E. Lang, M.J. Betenbaugh, J.D. Young, The impact of anti-apoptotic gene Bcl-2 expression on CHO central metabolism, Metab. Eng. 25 (2014) 92–102.
[2] B. Dionne, N. Mishra, M. Butler, A low redox potential affects monoclonal antibody assembly and glycosylation in cell culture, J. Biotechnol. 246 (2017) 71–80.
[3] A.M. Lewis, W.D. Croughan, N. Aranibar, A.G. Lee, B. Warrack, N.R. Abu-Absi, R. Patel, B. Drew, M.C. Borys, M.D. Reily, Z.J. Li, Understanding and controlling sialylation in a CHO fc-fusion process, PLoS One 11 (2016) e0157111.
[4] C.A. Orellana, E. Marcellin, R.W. Palfreyman, T.P. Munro, P.P. Gray, L.K. Nielsen, RNA-Seq highlights high clonal variation in monoclonal antibody producing CHO cells, Biotechnol. J. 13 (2017) 1700231.
[5] H.H. Hsu, M. Araki, M. Mochizuki, Y. Hori, M. Murata, P. Kahar, T. Yoshida, T. Hasunuma, A. Kondo, A systematic approach to time-series metabolite profiling and RNA-seq analysis of Chinese hamster ovary cell culture, Sci. Rep. 7 (2017) 43518.
[6] N. Alden, R. Raju, K. McElearney, J. Lambropoulos, R. Kshirsagar, A. Gilbert, K. Lee, Using metabolomics to identify cell line-independent indicators of growth inhibition for Chinese hamster ovary cell-based bioprocesses, Metabolites 10 (2020) 199.
[7] Z. Huang, J. Xu, A. Yongky, C.S. Morris, A.L. Polanco, M. Reily, M.C. Borys, Z.J. Li, S. Yoon, CHO cell productivity improvement by genome-scale modeling and pathway analysis: application to feed supplements, Biochem. Eng. J. 160 (2020) 107638.
[8] Z. Huang, S. Yoon, Integration of time-series transcriptomic data with genome-scale CHO metabolic models for mAb engineering, Processes 8 (2020) 331.
[9] C. Morris, A. Polanco, A. Yongky, J. Xu, Z. Huang, J. Zhao, K.S. McFarland, S. Park, B. Warrack, M. Reily, M.C. Borys, Z. Li, S. Yoon, Bigdata analytics identifies metabolic inhibitors and promoters for productivity improvement and optimization of monoclonal antibody (mAb) production process, Bioresour. Bioprocess. 7 (2020) 31.
[10] S. Sha, H. Bhatia, S. Yoon, An RNA-seq based transcriptomic investigation into the productivity and growth variants with Chinese hamster ovary cells, J. Biotechnol. 271 (2018) 37–46.
[11] F.N.K. Yusufi, M. Lakshmanan, Y.S. Ho, B.L.W. Loo, P. Ariyaratne, Y. Yang, S.K. Ng, T.R.M. Tan, H.C. Yeo, H.L. Lim, S.W. Ng, A.P. Hiu, C.P. Chow, C. Wan, S. Chen, G. Teo, G. Song, J.X. Chin, X. Ruan, K.W.K. Sung, W.S. Hu, M.G.S. Yap, M. Bardor, N. Nagarajan, D.Y. Lee, Mammalian systems biotechnology reveals global cellular adaptations in a recombinant CHO cell line, Cell Syst. 4 (2017) 530–542, e536.
[12] J.A.H. Bort, M. Hackl, H. Hoflmayer, V. Jadhav, E. Harreither, N. Kumar, W. Ernst, J. Grillari, N. Borth, Dynamic mRNA and miRNA profiling of CHO-K1 suspension cell cultures, Biotechnol. J. 7 (2012) 500–515.
[13] R. Korke, M.D.L. Gatti, A.L.Y. Lau, J.W.E. Lim, T.K. Seow, M.C.M. Chung, W.-S. Hu, Large scale gene expression profiling of metabolic shift of mammalian cells in culture, J. Biotechnol. 107 (2004) 1–17.
[14] H. Le, N. Vishwanathan, A. Kantardjieff, I. Doo, M. Srienc, X. Zheng, N. Somia, W. S. Hu, Dynamic gene expression for metabolic engineering of mammalian cells in culture, Metab. Eng. 20 (2013) 212–220.
[15] C. Chen, H. Le, C.T. Goudar, An automated RNA-Seq analysis pipeline to identify and visualize differentially expressed genes and pathways in CHO cells, Biotechnol. Prog. 31 (2015) 1150–1162.
[16] C. Chen, H. Le, C.T. Goudar, Evaluation of two public genome references for Chinese hamster ovary cells in the context of rna-seq based gene expression analysis, Biotechnol. Bioeng. 114 (2017) 1603–1613.
[17] Y.K. Gowtham, C.A. Saski, S.W. Harcum, Low glucose concentrations within typical industrial operating conditions have minimal effect on the transcriptome of recombinant CHO cells, Biotechnol. Prog. 33 (2017) 771–785.
[18] J.H. Lee, Y.R. Jeong, Y.G. Kim, G.M. Lee, Understanding of decreased sialylation of Fc-fusion protein in hyperosmotic recombinant Chinese hamster ovary cell culture: N-glycosylation gene expression and N-linked glycan antennary profile, Biotechnol. Bioeng. 8 (2017) 1721–1732.
[19] S.M. Lee, Y.G. Kim, E.G. Lee, G.M. Lee, Digital mRNA profiling of N-glycosylation gene expression in recombinant Chinese hamster ovary cells treated with sodium butyrate, J. Biotechnol. 171 (2014) 56–60.

[20] S. Sha, C. Agarabi, K. Brorson, D.Y. Lee, S. Yoon, N-glycosylation design and control of therapeutic monoclonal antibodies, Trends Biotechnol. 34 (2016) 835–846.
[21] T.K. Ha, Y.G. Kim, G.M. Lee, Understanding of altered N-glycosylation-related gene expression in recombinant Chinese hamster ovary cells subjected to elevated ammonium concentration by digital mRNA counting, Biotechnol. Bioeng. 112 (2015) 1583–1593.
[22] M.-A. Rodrigo, D.A. J, Multiplexed digital mRNA expression analysis profiles system-wide changes in mRNA abundance and responsiveness of UPR-specific gene expression changes during batch culture of recombinant Chinese hamster ovary cells, Biotechnol. J. 13 (2018) 1700429.
[23] J. Feichtinger, I. Hernandez, C. Fischer, M. Hanscho, N. Auer, M. Hackl, V. Jadhav, M. Baumann, P.M. Krempl, C. Schmidl, M. Farlik, M. Schuster, A. Merkel, A. Sommer, S. Heath, D. Rico, C. Bock, G.G. Thallinger, N. Borth, Comprehensive genome and epigenome characterization of CHO cells in response to evolutionary pressures and over time, Biotechnol. Bioeng. 113 (2016) 2241–2253.
[24] I. Hernandez, H. Dhiman, G. Klanert, V. Jadhav, N. Auer, M. Hanscho, M. Baumann, A. Esteve-Codina, M. Dabad, J. Gomez, T. Alioto, A. Merkel, E. Raineri, S. Heath, D. Rico, N. Borth, Epigenetic regulation of gene expression in Chinese hamster ovary cells in response to the changing environment of a batch culture, Biotechnol. Bioeng. 116 (2019) 677–692.
[25] A. Kucukural, N. Merowsky, M. Garber, Debrowser: debrowser: Interactive Differential Expresion Analysis Browser, R package version 1.2.4, 2016. https://github.com/UMMS-Biocore/debrowser.
[26] E. Eden, R. Navon, I. Steinfeld, D. Lipson, Z. Yakhini, GOrilla: a tool for discovery and visualization of enriched GO terms in ranked gene lists, BMC Bioinformatics 10 (2009) 1–7.
[27] D. Trachootham, W. Lu, M.A. Ogasawara, R.D. Nilsa, P. Huang, Redox regulation of cell survival, Antioxid. Redox Signal. 10 (2008) 1343–1374.
[28] B.C. Mulukutla, A. Yongky, T. Le, D.G. Mashek, W.S. Hu, Regulation of glucose metabolism - a perspective from cell bioprocessing, Trends Biotechnol. 34 (2016) 638–651.
[29] B.C. Mulukutla, A. Yongky, S. Grimm, P. Daoutidis, W.S. Hu, Multiplicity of steady states in glycolysis and shift of metabolic state in cultured mammalian cells, PLoS One 10 (2015) e0121561.
[30] B.C. Mulukutla, S. Khan, A. Lange, W.S. Hu, Glucose metabolism in mammalian cell culture: new insights for tweaking vintage pathways, Trends Biotechnol. 28 (2010) 476–484.
[31] W.S. Ahn, M.R. Antoniewicz, Metabolic flux analysis of CHO cells at growth and non-growth phases using isotopic tracers and mass spectrometry, Metab. Eng. 13 (2011) 598–609.
[32] S. Selvarasu, Y. Kim do, I.A. Karimi, D.Y. Lee, Combined data preprocessing and multivariate statistical analysis characterizes fed-batch culture of mouse hybridoma cells for rational medium design, J. Biotechnol. 150 (2010) 94–100.
[33] S. Selvarasu, V.V. Wong, I.A. Karimi, D.Y. Lee, Elucidation of metabolism in hybridoma cells grown in fed-batch culture by genome-scale modeling, Biotechnol. Bioeng. 102 (2009) 1494–1504.
[34] W.S. Ahn, M.R. Antoniewicz, Towards dynamic metabolic flux analysis in CHO cell cultures, Biotechnol. J. 7 (2012) 61–74.
[35] A.A. Sablina, A.V. Budanov, G.V. Ilyinskaya, L.S. Agapova, J.E. Kravchenko, P. M. Chumakov, The antioxidant function of the p53 tumor suppressor, Nat. Med. 11 (2005) 1306–1313.
[36] K.E. Wellen, C.B. Thompson, Cellular metabolic stress: considering how cells respond to nutrient excess, Mol. Cell 40 (2010) 323–332.
[37] Y. Gao, S. Ray, S. Dai, A.R. Ivanov, N.R. Abu-Absi, A.M. Lewis, Z. Huang, Z. Xing, M.C. Borys, Z.J. Li, B.L. Karger, Combined metabolomics and proteomics reveals hypoxia as a cause of lower productivity on scale-up to a 5000-liter CHO bioprocess, Biotechnol. J. 11 (2016) 1190–1200.
[38] K. Brand, Aerobic glycolysis by proliferating cells: protection against oxidative stress at the expense of energy yield, J. Bioenerg. Biomembr. 29 (1997) 335–364.
[39] N. Sengupta, S.T. Rose, J.A. Morgan, Metabolic flux analysis of CHO cell metabolism in the late non-growth phase, Biotechnol. Bioeng. 108 (2011) 82–92.
[40] S.P. Hussain, P. Amstad, P. He, A. Robles, S. Lupold, I. Kaneko, M. Ichimiya, S. Sengupta, L. Mechanic, S. Okamura, L.J. Hofseth, M. Moake, M. Nagashima, K. S. Forrester, C.C. Harris, p53-induced up-regulation of MnSOD and GPx but not catalase increases oxidative stress and apoptosis, Cancer Res. 64 (2004) 2350–2356.
[41] K. Shirato, N. Kazuki, K. Hiroaki, T. Shinji, G. Congxiao, T. Angata, K. Ohtsubo, N. Taniguchi, Hypoxic regulation of glycosylation via the N acetylglucosamine cycle, J. Clin. Biochem. Nutr. 48 (2011) 20–25.
[42] N. Kochanowski, F. Blanchard, R. Cacan, F. Chirat, E. Guedon, A. Marc, J. L. Goergen, Intracellular nucleotide and nucleotide sugar contents of cultured CHO cells determined by a fast, sensitive, and high-resolution ion-pair RP-HPLC, Anal. Biochem. 348 (2006) 243–251.
[43] T.K. Villiger, R.F. Steinhoff, M. Ivarsson, T. Solacroup, M. Stettler, H. Broly, J. Krismer, M. Pabst, R. Zenobi, M. Morbidelli, M. Soos, High-throughput profiling of nucleotides and nucleotide sugars to evaluate their impact on antibody N-glycosylation, J. Biotechnol. 229 (2016) 3–12.
[44] P.M. Jedrzejewski, I.J. del Val, A. Constantinou, A. Dell, S.M. Haslam, K.M. Polizzi, C. Kontoravdi, Towards controlling the glycoform: a model framework linking extracellular metabolites to antibody glycosylation, Int. J. Mol. Sci. 15 (2014) 4492–4522.
[45] S. Sha, S. Yoon, An investigation of nucleotide sugar dynamics under the galactose supplementation in CHO cell culture, Process. Biochem. 81 (2019) 165–174.
[46] B.C. Mulukutla, M. Gramer, W.S. Hu, On metabolic shift to lactate consumption in fed-batch culture of mammalian cells, Metab. Eng. 14 (2012) 138–149.
[47] F. Hartley, T. Walker, V. Chung, K. Morten, Mechanisms driving the lactate switch in Chinese hamster ovary cells, Biotechnol. Bioeng. 115 (2017) 1890–1903.
[48] F. Zagari, M. Jordan, M. Stettler, H. Broly, F.M. Wurm, Lactate metabolism shift in CHO cell culture: the role of mitochondrial oxidative activity, N. Biotechnol. 30 (2013) 238–245.
[49] T.M. Sauerwald, B. Figueroa Jr., J.M. Hardwick, G.A. Oyler, M.J. Betenbaugh, Combining caspase and mitochondrial dysfunction inhibitors of apoptosis to limit cell death in mammalian cell cultures, Biotechnol. Bioeng. 94 (2006) 362–372.
[50] H. Dorai, Y.S. Kyung, D. Ellis, C. Kinney, C. Lin, D. Jan, G. Moore, M.J. Betenbaugh, Expression of anti-apoptosis genes alters lactate metabolism of Chinese hamster ovary cells in culture, Biotechnol. Bioeng. 103 (2009) 592–608.